Chemical Science

EDGE ARTICLE

View Article Online
View Journal | View Issue

Cite this: *Chem. Sci.*, 2016, **7**, 4468

Multivalence cooperativity leading to "all-or-nothing" assembly: the case of nucleation-growth in supramolecular polymers†

Elkin Lopez-Fontal,[a] Lilia Milanesi[b] and Salvador Tomas*[a]

All-or-nothing molecular assembly events, essential for the efficient regulation of living systems at the molecular level, are emerging properties of complex chemical systems that are largely attributed to the cooperativity of weak interactions. The link between the self-assembly and the interactions responsible for the assembly is however often poorly defined. In this work we demonstrate how the chelate effect (multivalence cooperativity) can play a central role in the regulation of the all-or-nothing assembly of structures (supramolecular polymers here), even if the building blocks are not multivalent. We have studied the formation of double-stranded supramolecular polymers formed from Co-metalloporphyrin and bi-pyridine building blocks. Their cooperative nucleation–elongation assembly can be summarized as a thermodynamic cycle, where the monomer weakly oligomerizes linearly or weakly dimerizes laterally. But thanks to the chelate effect, the lateral dimer readily oligomerizes linearly and the oligomer readily dimerizes laterally, leading to long double stranded polymers. A model based on this simple thermodynamic cycle can be applied to the assembly of polymers with any number of strands, and allows for the determination of the length of the polymer and the all-or-nothing switching concentration from the pairwise binding constants. The model, which is consistent with the behaviour of supramolecular polymers such as microtubules and gelators, clearly shows that all-or-nothing assembly is triggered by a change in the mode of assembly, from non-multivalent to multivalent, when a critical concentration is reached. We believe this model is applicable to many molecular assembly processes, ranging from the formation of cell–cell focal adhesion points to crystallization.

Received 2nd February 2016
Accepted 18th March 2016

DOI: 10.1039/c6sc00520a

www.rsc.org/chemicalscience

Introduction

The regulation of biological systems at the molecular level requires that molecular assembly events respond efficiently to changes in the environment. This responsiveness often rests on the amplification of an input signal (for example, a change in temperature, or the presence of a particular chemical), that leads to an all-or-nothing switch between assembled and de-assembled states. The amplification of the input signal is an emerging property of the system, and can be attributed to the positive cooperativity between the intermolecular interactions involved, resulting in increased stability (above the simple addition of all the pairwise interactions) of assemblies held by multiple interactions.[1,2] Cooperativity can be classified as allosteric cooperativity and chelate cooperativity, also termed multivalence cooperativity. In the first, initial binding events lead to changes in the assembled molecules (such as polarization of H-bond donors or conformational changes) that make the binding of additional molecules more efficient. In chelate cooperativity, the formation of the first interaction between two molecules pays the entropic cost of bringing the molecules together, making any subsequent interaction more stable.[3–5]

The linear assembly of molecules leads to the formation of supramolecular polymers, which in biomolecular systems are involved in many vital cellular processes, including cell division (microtubules) or cell motion (actin filaments).[6] Supramolecular polymers are also of interest for technological and biomedical applications.[7,8] For example, supramolecular polymers produced by the self-assembly of small synthetic molecules have properties that are tuneable through using different components and are interesting for the development of opto-electronic devices.[9–11] The crosslinking of nano-filaments leads to the formation of small molecule based gels, with applications ranging from drug delivery to tissue engineering.[12–18]

[a]*Institute of Structural and Molecular Biology and Department of Biological Sciences, School of Science, Birkbeck University of London, Malet Street, London WC1E 7HX, UK. E-mail: s.tomas@bbk.ac.uk*

[b]*School of Biological and Chemical Sciences, Queen Mary University of London, Mile End Road, London E1 4NS, UK*

† Electronic supplementary information (ESI) available: Experimental methods, including sample preparation for NMR, UV and electron microscopy experiments, the building up of the X-ray derived dimer structure, analysis of the binding of monovalent ligands, additional data on binding constant determination, effect of buffer concentration on polymer dimerization and detailed derivation of the equations. See DOI: 10.1039/c6sc00520a

In supramolecular polymerization, especially for biological examples such as microtubules, assembly of the building blocks may take place in a cooperative fashion, in what is termed a nucleation–elongation mechanism. This cooperative effect can be quantified,[19,20] and has been often explained in terms of allosteric cooperativity, whereby after a few molecules form the nucleus, conformational changes take place that enhance the interaction of subsequent molecules.[21–24]

The chelate effect, normally seen as a property of complexes formed between two molecules held together by multiple interactions, has not been attributed an explicit role in the assembly of supramolecular polymers, except for the special case of helical polymers.[19,25,26] Yet, in most cases, supramolecular polymers are formed by bundles of several strands. Within such structures, the assembly can be interpreted as the combination of two molecular recognition processes: the longitudinal growth of each strand and the lateral assembly between the strands. The latter involves the simultaneous lateral interaction of many building blocks and it is therefore subject to a multivalence cooperativity effect. In other words, the nucleation step would yield a multivalent nucleus, resulting in the amplification of the polymerization process thanks to the chelate effect. Here we study the assembly of a polymer formed from two different building blocks: a cobalt metalloporphyrin and 4,4′-bipyridine. Porphyrin-containing assemblies are intrinsically interesting as they have potential applications for light-harvesting and the development of nano-wires.[27–29] In the present work we take advantage of the favourable spectroscopic properties of porphyrins[30,31] to carry out a detailed analysis of the role played by the chelate effect in supramolecular polymerization.

Results and discussion

Co metalloporphyrin **C** was prepared through the metalation of a free-base with cobalt acetate.[32] The sharp ^{1}H-NMR signals show that the metal center in **C** is diamagnetic Co(III) rather than paramagnetic Co(II). The ^{1}H-NMR spectrum of porphyrin **C** in aqueous buffers (sodium phosphate, 5 to 100 mM, pH 7.2) is independent of the concentration up to 3 mM in our experiments, consistent with the absence of self-aggregation in these conditions. The addition of di-valent bipyridine (**B**) to di-valent porphyrin **C** at concentrations between 25 and 200 μM leads to changes in the ^{1}H-NMR spectrum that are consistent with the formation of small oligomeric species with alternating **CB** building blocks (Fig. 1). Diffusion NMR experiments, together with the changes in the ^{1}H-NMR signal intensity with changing **C**/**B** ratios, allowed for the identification of the presence of complexes **CB**, $\mathbf{CB_2}$, $\mathbf{C_2B}$, $\mathbf{C_2B_2}$ and $\mathbf{C_2B_3}$ (Fig. 2A) (see the ESI, Fig. S1 and Table S1† for details).[33] K_1, K_2 and K_3 are the stepwise binding constants for the formation of **CB**, $\mathbf{CB_2}$ and $\mathbf{C_2B}$, *i.e.*

$$K_1 = \frac{[\mathbf{CB}]}{[\mathbf{C}][\mathbf{B}]} \quad (1)$$

$$K_2 = \frac{[\mathbf{CB_2}]}{[\mathbf{CB}][\mathbf{B}]} \quad (2)$$

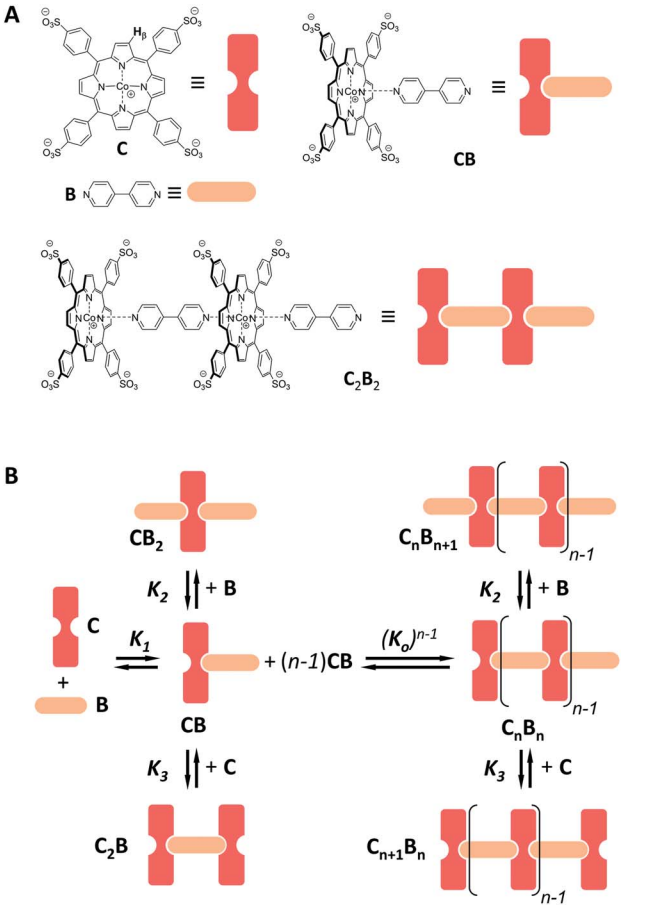

Fig. 1 (A) Chemical structure of **C** and **B** and of choice complexes, together with their cartoon representations. The β hydrogen of **C** (whose ^{1}H-NMR signal is followed in the NMR experiments) is highlighted. (B) Schematic representation of the oligomerization equilibria.

$$K_3 = \frac{[\mathbf{C_2B}]}{[\mathbf{CB}][\mathbf{C}]} \quad (3)$$

K_1, K_2 and K_3 were determined by integration of the corresponding ^{1}H-NMR peaks. K_1 and K_2 calculated using UV titration are in agreement with the values derived from the NMR data (Fig. S2† and Table 1). All binding events involving **C** and **B** can be expressed as a function of K_1, K_2 and K_3. For example, the oligomerization constant of the **CB** repeats can be written as (Fig. 1B, see the ESI† for details):

$$K_o = \frac{[\mathbf{C}_n\mathbf{B}_n]}{[\mathbf{C}_{n-1}\mathbf{B}_{n-1}][\mathbf{CB}]} = \frac{4(K_2K_3)}{K_1} \quad (4)$$

Eqn (1)–(4) in combination with the mass balance allow for the modelling of the distribution of species observed in the NMR experiments (Fig. 2A and B). For a mixture of **C** and **B** in a 1 to 1 ratio, the length of the oligomer can be expressed by the average number of **CB** repeats $\langle N\rangle$, calculated as follows (see the ESI† for details):

$$\langle N\rangle = \frac{1}{1 - 4K_2K_3[\mathbf{C}][\mathbf{B}]} \quad (5)$$

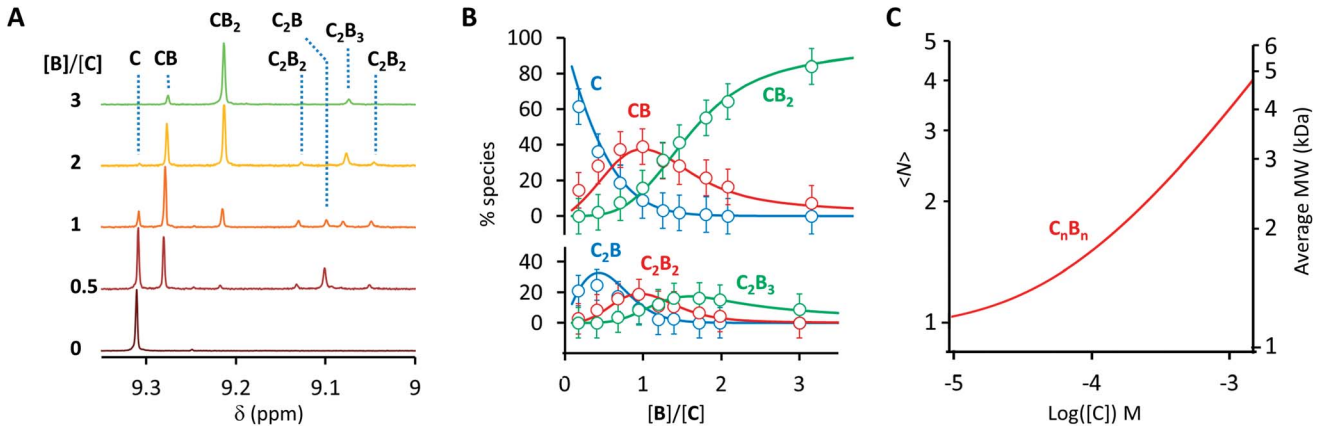

Fig. 2 (A) Section of the ^{1}H-NMR spectra of mixtures of **B** and **C**, showing the signal assigned to the β hydrogen of the porphyrin ring. The concentration of **C** is 100 μM in all cases. (B) Speciation plot showing the amount of the various $\mathbf{C}_n\mathbf{B}_n$ species as a function of the [**B**]/[**C**] ratio determined by integration of the ^{1}H-NMR signals (circles) and modelled using the values of K_1, K_2 and K_3 listed in Table 1 (continuous lines). The error bars are based on the intrinsic error of the NMR integral (*ca.* 10%). (C) Changes in the average number of **CB** repeats (*i.e.*, $\langle N \rangle$) and average molecular weight of an oligomer $\mathbf{C}_n\mathbf{B}_n$ as a function of the total concentration of **C** (with [**C**] = [**B**]), estimated using the equilibria depicted in Fig. 1B and the values of K_1, K_2 and K_3 listed in Table 1.

$\langle N \rangle$ increases steadily as the concentration of the building blocks increases, typical of an isodesmic oligomerization (Fig. 2C). The NMR data at concentrations of building blocks above 100 μM does however contradict this expectation. For example, according to our model, for concentrations of **C** and **B** of 1 mM the dominant species should be an oligomer with 3–4 **CB** repeats, with a MW of just below 5000 Da (Fig. 2C). In practice, the ^{1}H-NMR signals disappear, indicating the presence of very large oligomers (*i.e.* polymers) (Fig. 3A). This sudden increase in the linear assembly size is attributed to a cooperative effect that is not accounted for in the modelling.

At concentrations when the ^{1}H-NMR signals start decreasing (*i.e.*, above 100 μM) a new, red-shifted Soret band appears in the UV spectrum (Fig. 3A and B). Red-shifted Soret bands are indicative of the formation of J-type aggregates between porphyrin rings, where the rings are stacked in a staggered fashion.[34,35] A possible arrangement that could lead to a J-type aggregate is a dimer of polymers. In the dimer, porphyrin rings intercalate in the space between the two rings of a second polymer, driven by the hydrophobic effect (Fig. 3C).

A number of additional experimental results support this interpretation: (i) crystal structures of **C**–**B** complexes described in the literature show the same arrangement (Fig. 3C; see also the ESI and Fig. S3†);[36] (ii) electron microscopy experiments, which show the presence of needle-like structures with a thickness that is consistent with the width of the dimeric oligomer (Fig. 3D and S4†) and (iii) the addition of salt to mixtures of **C** and **B** at low concentrations, which triggers the rise of the red-shifted band in the UV spectrum (Fig. S5†). With K_1, K_2 and K_3 (and therefore K_o) independent of the salt concentration (see Table 1 and S2†) this behaviour is attributed to the decrease in the electrostatic repulsion between polymers bearing multiple anionic moieties at higher ionic strength, favouring their dimerization. Changes in the ^{1}H-NMR and UV spectra when the concentration of **C** and **B** is around 1 mM can be modelled if we take into account the dimerization of the polymers, leading to the double-stranded polymers $(\mathbf{C}_n\mathbf{B}_n)_2$, with the lateral association constant K_{nl} (Fig. 4A)

$$K_{nl} = \frac{\left[(\mathbf{C}_n\mathbf{B}_n)_2\right]}{\left[\mathbf{C}_n\mathbf{B}_n\right]^2} \quad (6)$$

In each strand, the repeating unit **CB** can be seen as a binding site, so that dimerization of the polymer results from the binding of two multivalent single-stranded polymers. K_{nl} can therefore be expressed as a function of 3 parameters: a lateral association constant per unit repeat (*i.e.*, **CB**), K_l, the effective molarity EM, a parameter that gives a measure of the local concentration of complementary binding sites in a complex held by multiple interactions, and the number of polymer repeats n in each of the strands:

$$K_{nl} = \mathrm{EM}^{n-1} K_l^{\,n} \quad (7)$$

Table 1 Binding parameters[a]

	K_1	K_2	K_3	K_o
UV	$1.1 \times 10^6 \pm 1.2 \times 10^5$	$9.7 \times 10^4 \pm 1.6 \times 10^4$	nd	nd
NMR	$1.1 \times 10^6 \pm 2.6 \times 10^4$	$1.0 \times 10^5 \pm 2.0 \times 10^4$	$2.3 \times 10^4 \pm 6.0 \times 10^3$	$8.4 \times 10^3 \pm 3.2 \times 10^3$

[a] The units for the binding constants are M^{-1} in all cases. The quoted error is twice the standard deviation of the mean.

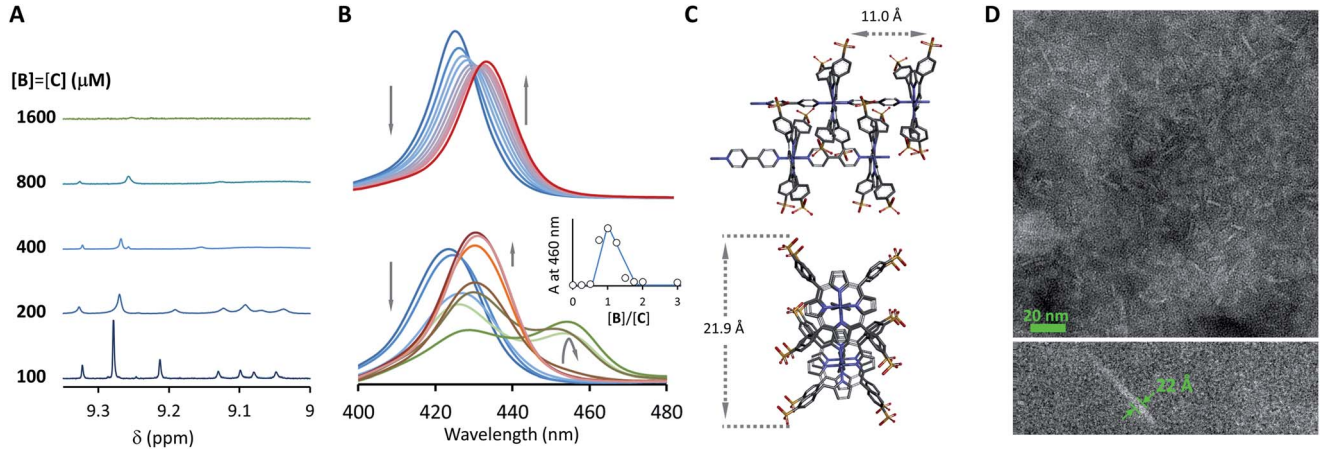

Fig. 3 Evidence of polymer dimerization. (A) Changes in the ^{1}H NMR signal assigned to the β proton of **C** as the concentration of the building blocks increases. The buffer used is 5 mM sodium phosphate, pH 7.20. (B) Changes in the Soret band of the UV spectrum of **C** as the [**B**]/[**C**] ratio changes from 0 to 3 in phosphate buffer, 5 mM, pH 7.20. In the top panel the concentration of **C** was 50 μM and in the bottom panel it was 400 μM. The inset shows the changes in absorbance at 460 nm for the lower panel experiment (empty circles) and the fit to a polymer dimerization model (blue line). (C) 3D model of the dimeric form $(\mathbf{C}_n\mathbf{B}_n)_2$ of the oligomer $\mathbf{C}_n\mathbf{B}_n$, based on the crystal structure reported in ref. 34 (see the ESI† for details). (D) Negative stain TEM image of a mixture of **C** : **B** in a ratio 1 to 1. The bottom section shows the zoom-in to an isolated single fibre together with the estimated width. The average thickness of the needle-like features is 22 ± 2 A (at a 95% confidence level, see the ESI† for details).

For the oligomerization of **C** and **B**, the formation of three types of oligomers is taken into account (**B** capped, **C** capped and with mixed capping, see Fig. 1B). For the dimerization of the polymer we make two assumptions that considerably simplify the system (Fig. 4A): (i) only mixed capping polymers exist (*i.e.*, with equal **C** and **B** units). This assumption is supported by the fact that, for polymers, the average **C**/**B** ratio is equal to 1. (ii) The initial concentration of complex **CB**, $[\mathbf{CB}]_0$, is dictated solely by K_1. This assumption is supported by the fact that K_1 is much larger than all the other association constants (Table 1). Therefore we view the polymerization process as the assembly of equal **CB** monomers. We call the concentration of **B** and **C** that are not involved in the formation of **CB** $[\mathbf{B}]_x$ and $[\mathbf{C}]_x$, respectively. The polymer can be disassembled by the addition of excess **B**, that is, increasing $[\mathbf{B}]_x$ (leading to $\mathbf{CB}_2$) or **C**, that is, increasing $[\mathbf{C}]_x$ (leading to $\mathbf{C}_2\mathbf{B}$), as dictated by K_2 and K_3, respectively (Fig. 4A). The equation that relates all the concentrations is (see the ESI† for the detailed derivation):

$$[\mathbf{CB}]_0 = \frac{K_2[\mathbf{CB}][\mathbf{B}]_x}{(1+K_2[\mathbf{CB}])} + \frac{K_3[\mathbf{CB}][\mathbf{C}]_x}{(1+K_3[\mathbf{CB}])} + \frac{[\mathbf{CB}]}{(1-K_o[\mathbf{CB}])^2} + \frac{2K_1[\mathbf{CB}]^2}{\left(1-K_1\mathrm{EM}K_o^2[\mathbf{CB}]^2\right)^2} \quad (8)$$

where the first two members are the equilibrium concentrations of $\mathbf{CB}_2$ and $\mathbf{C}_2\mathbf{B}$, the third member is the concentration of **CB** repeating units within a single stranded oligomer of any length and the fourth member is the concentration of **CB** units within double stranded polymers of any length. Eqn (8), combined with the mass balance (eqn (S45) and (S46)†), allows for the calculation of the concentration of free **CB** and therefore of all the species, including that of the polymer dimer $(\mathbf{C}_n\mathbf{B}_n)_2$, at any initial concentration of the building blocks (Fig. S6†). Eqn (8) also shows that for the polymer dimer to form to any meaningful extent, (*i.e.*, for multivalence cooperativity to be positive) the product K_1EM must be larger than 1.[2] Around 460 nm the absorbance A in the UV spectrum is solely due to the red-shifted band assigned to the polymer dimer, $(\mathbf{C}_n\mathbf{B}_n)_2$, and can be written as (see the ESI† for details):

$$A = \varepsilon \frac{2K_1[\mathbf{CB}]^2}{\left(1-K_1\mathrm{EM}K_o^2[\mathbf{CB}]^2\right)^2} \quad (9)$$

where ε is the molar extinction coefficient per **CB** unit at the wavelength under study (Fig. 3B). With all the constants independently determined, except for K_1 and EM, the model fits remarkably well to the experimental changes in absorbance at 460 nm (Fig. 3B), further supporting the polymer-dimer model. Using a value of the EM of 1 M, (a reasonable value in supramolecular systems[37]) the fitting produced a K_1 value of 6.1 M^{-1} in sodium phosphate, 5 mM, pH 7.20. The constant is small, but due to multivalence cooperativity the polymers dimerize quantitatively. As a consequence, there is a sudden increase in the population of large double-stranded polymers when a critical concentration is reached (Fig. 4B). The average number of repeat units in the double-stranded polymer, $\langle N_2 \rangle$, can be calculated from the concentration of the complex **CB** as follows:

$$\langle N_2 \rangle = \frac{1}{1-K_o^2\mathrm{EM}K_1[\mathbf{CB}]^2} \quad (10)$$

The changes in polymer length (and therefore molecular weight) predicted by eqn (10) are consistent with the changes in the ^{1}H NMR spectrum, where the rapid rise in the polymer average molecular weight and the increase in the overall large

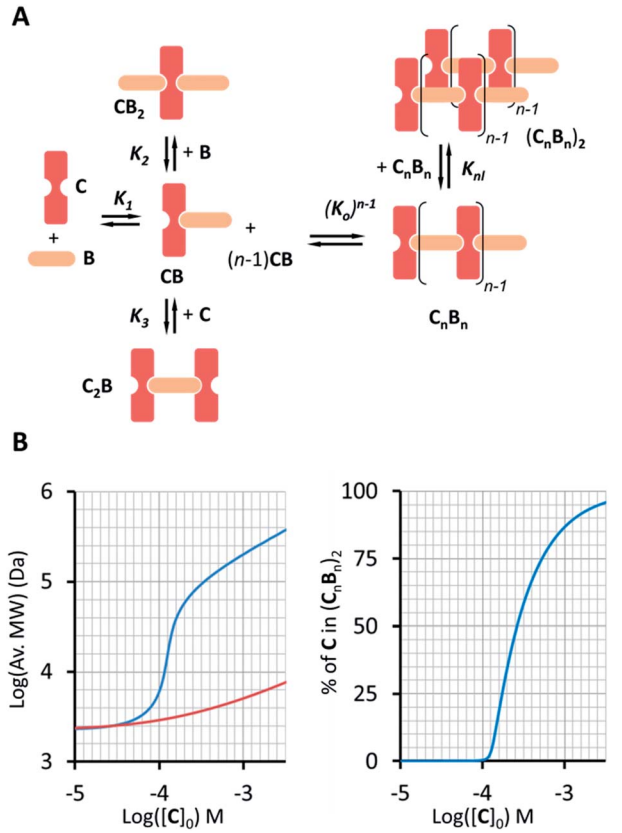

Fig. 4 (A) Equilibria that describe the oligomer dimerization model. (B) Left panel: changes in the average MW of the oligomer dimer $(\mathbf{C}_n\mathbf{B}_n)_2$ (blue trace) as the total concentration of **C** increases ([B] = [C]). For comparison, the increase in the average oligomer molecular weight in the absence of dimerization is also shown (red trace). The right panel shows the change in the percentage of **C** in $(\mathbf{C}_n\mathbf{B}_n)_2$ as a function of the total concentration of **C**.

polymer population leads to the line broadening observed (Fig. 3A and 4).

Our model, which accounts for the formation of a double-stranded polymer, can be expanded to the formation of multi-stranded polymers with m strands. Unlike the number of polymer repeats n, which can be very large, m is a discrete number. For simplicity and general applicability, we consider that the polymers are formed by the self-assembly of only one type of building block, that we call **M**, rather than the two components **C** and **B**. Monomer **M** can assemble in the longitudinal direction, forming single stranded polymers of n units $\mathbf{M}_n$ (Fig. 5A, equilibrium 1). The assembly is isodesmic, with the oligomerization constant K_o. The single strand $\mathbf{M}_n$ can interact laterally with up to another $m-1$ strands to form a multi-stranded polymer of m strands $(\mathbf{M}_n)_m$. The lateral assembly is also isodesmic, with the lateral association constant $K_{nl} = K_l^n \mathrm{EM}^{n-1}$, according to eqn (5) (Fig. 5A, equilibrium 4). We can depict an alternative mechanism for the formation of polymers with m strands $(\mathbf{M}_n)_m$, with **M** first assembling laterally with up to $m-1$ molecules of **M** to produce the complex $\mathbf{M}_m$, following an isodesmic mechanism with the stepwise lateral assembly constant K_l (Fig. 5A, equilibrium 2). The complex $\mathbf{M}_m$ then assembles linearly with another $n-1$ $\mathbf{M}_m$ complexes, following an isodesmic mechanism with the stepwise oligomerization constant K_{mo}, which is related to K_o as follows:

$$K_{mo} = K_o{}^m \mathrm{EM}^{m-1} \tag{11}$$

In other words, **M** can assemble in two orthogonal directions, but the lateral assembly ends at a relatively small number for m while the longitudinal assembly is open ended (Fig. 5A). Irrespective of the route of formation of the multi-stranded polymer, the expression that relates $[\mathbf{M}]_0$ and $[\mathbf{M}]$ for a polymer composed of a bundle of m strands can be written as:

$$[\mathbf{M}]_0 = \sum_{i=1}^{i=m} \frac{i K_l{}^{i-1} [\mathbf{M}]^i}{\left(1 - K_o{}^i \mathrm{EM}^{i-1} K_l{}^{i-1} [\mathbf{M}]^i\right)^2} \tag{12}$$

and the average number of $\mathbf{M}_i$ unit repeats (with i values from 1 to m) in a multi-stranded polymer with i strands, $\langle N_i \rangle$, is (see the ESI† for the detailed derivation of the equation):

$$\langle N_i \rangle = \frac{1}{1 - K_o{}^i \mathrm{EM}^{i-1} K_l{}^{i-1} [\mathbf{M}]^i} \tag{13}$$

Using eqn (12) and (13) and knowing K_o, the EM and K_l it is possible to determine the changes in the concentration of polymer bundles with any number of strands, and the average number of repeats in the polymer, as the total concentration of the monomer changes. These simulations reveal the following features of the system (Fig. 5): (i) the only species present to any meaningful extent are the monomer, short, single stranded oligomers and the multi-stranded polymer with a maximum number of strands m, while polymers with an i number of strands less than m form only to a very limited extent (Fig. 5B); (ii) the multi-stranded polymer forms following a typical nucleation-growth mechanism, appearing suddenly when a nucleation concentration is reached, with the polymer growing rapidly around this concentration (Fig. 5B and C); (iii) the preferred length of the polymer depends on the maximum number of strands m (Fig. 5C); and (iv) the onset of formation of the multi-stranded polymer is very sensitive to small variations in K_l or K_o (Fig. 5D).

The very high sensitivity of the multi-stranded polymer formation to subtle changes in either the pair-wise binding constants or the concentration of building block **M** is attributed to the fact that the system switches from the assembly of the monomer (equilibria 1 and 2, Fig. 5A) to the assembly of the nucleus, which is multivalent (equilibria 3 and 4, Fig. 5A) when a critical concentration of **M** is reached. However, it is not the multivalence on its own that provides the on–off assembly behaviour, but rather the fact that the nucleus is multivalent relative to the monomer. For example, a multivalent monomer **M′**, analogous to the nucleus $\mathbf{M}_m$, will yield polymers to the same extent as $\mathbf{M}_m$ (and to a much larger extent than **M**) but the assembly process will be isodesmic, showing a smooth dependence of the assembly on the concentration of **M′** (equilibrium 0, Fig. 5A and E). By contrast, for **M**, the assembly is dictated by

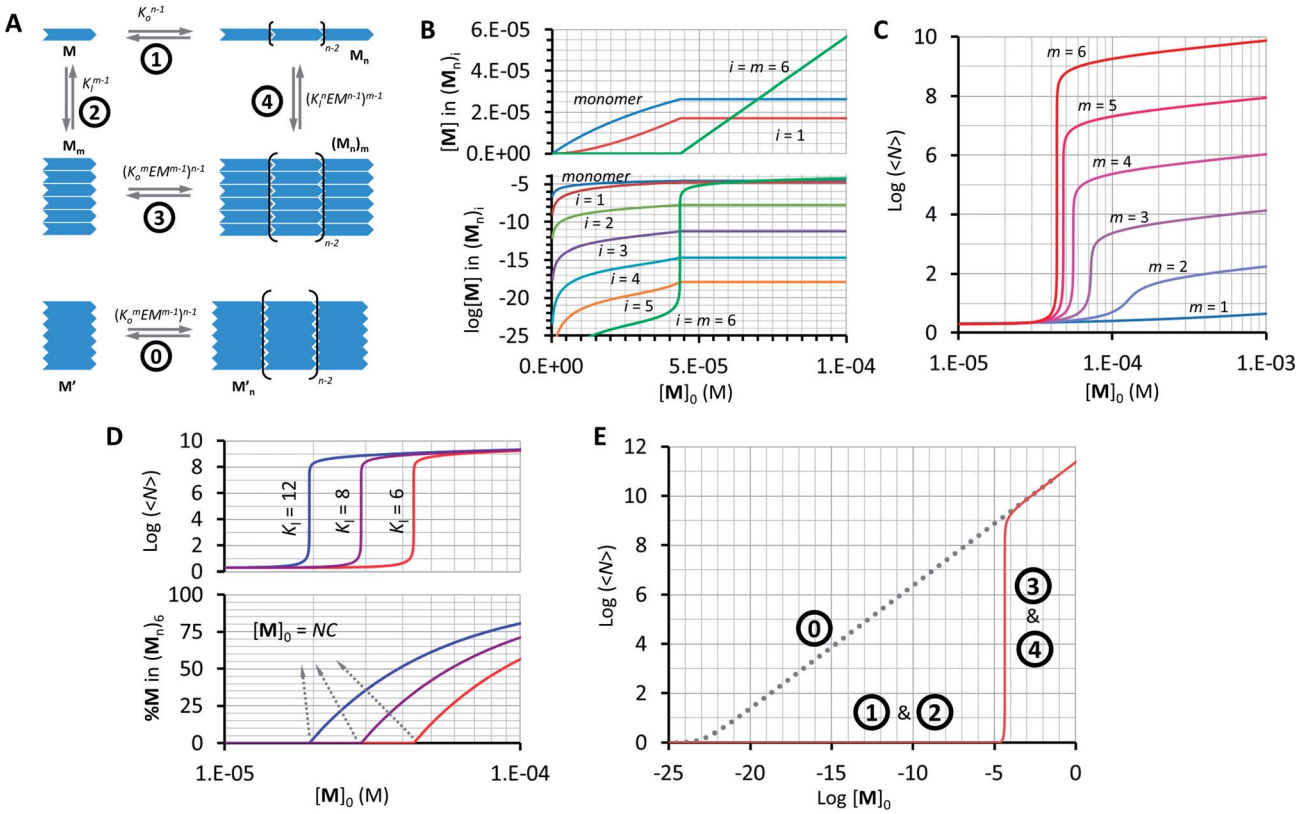

Fig. 5 Multi-stranded polymers. (A) Thermodynamic cycle for the formation of a multi-stranded polymer from **M** (1, 2, 3 and 4, top scheme) and the equilibrium for the oligomerization of **M′** (0, bottom scheme). (B) Changes in the concentration of building block **M** in the species of the form $(\mathbf{M}_n)_i$ as a function of the total concentration of **M**. A logarithmic scale on the *y*-axis is needed to show the changes in the concentration of multi-stranded polymers with $i < m$ (bottom panel). (C) Average number of repeats $\langle N \rangle$ in a multi-stranded polymer with a different maximum number of strands *m* as a function of the total monomer concentration, calculated using the multi-stranded polymer model. (D) Average number of repeats $\langle N \rangle$ (top) and percentage of the monomer (bottom) in a hexa-stranded polymer ($m = 6$) for different values of K_l and as a function of the total concentration of the monomer. (E) Changes in the average length of a hexa-stranded polymer as a function of the total concentration of **M′** (dotted line) and **M** (continuous line), the number labels show the dominating equilibrium according to panel A. The parameters used to generate these plots are $K_o = 8400\ M^{-1}$, $K'_o = (8400)^6\ M^{-1}$, $K_l = 6\ M^{-1}$ and EM = 1 M, except when stated in panel D.

the properties of $\mathbf{M}_m$ only above a certain critical concentration. At this concentration, the length and stability of the polymer formed from the assembly of **M** building blocks becomes comparable to that formed from **M′**, giving rise to a sudden increase in the concentration of the assembled species (Fig. 5A and E).

The switching point in the assembly regime occurs at the nucleation concentration, NC. The NC can be written as a function of the constants K_l and K_o, and the maximum number of strands *m* as follows (see the ESI† for the detailed derivation of the equation):

$$\mathrm{NC} = \frac{(K_l\mathrm{EM})^{1/m}}{K_l\mathrm{EM}K_o\left(1 - \frac{(K_l\mathrm{EM})^{1/m}}{K_l\mathrm{EM}}\right)^2} \quad (14)$$

Above the NC, the size of the oligomer can be expressed as a function of K_o, K_l, the EM and the number of strands *m* as follows:

$$\log\langle N_m\rangle = 0.5m \log K_o + 0.5(m-1)\log \mathrm{EM} - 0.5 \log m + 0.5 \log([\mathbf{M}]_0 - \mathrm{NC}) \quad (15)$$

A conveniently simple expression can be obtained by combining eqn (14) and (15) for the total concentration of the monomer which is twice that of the NC (see the ESI† for the detailed derivation of the equation):

$$\log\langle N_m\rangle = 0.5(m-1)\log K_o\mathrm{EM} - 0.5 \log m - 0.5\left(\frac{m-1}{m}\right)\log K_l\mathrm{EM} - \log\left(1 - (K_l\mathrm{EM})^{(1-m)/m}\right) \quad (16)$$

Eqn (16) allows for the calculation of the expected size of a multi-stranded polymer as a function of parameters that are characteristic of the monomer, that is, the association constants, the effective molarity and the number of strands in the polymer.

Conclusions

We have shown that the sequential assembly of cobalt metalloporphyrin **C** and 4,4′-bipyridine **B** leads to double stranded polymers, following a nucleation-growth mechanism. The mathematical model derived from the analysis of the spectroscopic data shows that the nucleation-growth mechanism is the consequence of a multivalence cooperative effect.

The model was applied to the assembly of multi-stranded polymers with any number of strands. Simulations show that this model accounts well for the all-or-nothing assembly typical of a nucleation-growth mechanism. The overall process can be summarized as a thermodynamic cycle. In the first part of the cycle, monomers assemble into nuclei, following an isodesmic mechanism. In the second part, the nuclei assemble into polymers, also following an isodesmic mechanism. The cooperative behaviour arises from the fact that the assembly of the nuclei is much more efficient than that of the monomers, on account of the multivalence effect. This model offers a simple interpretation of the all-or-nothing assembly observed in many natural (such as microtubules) and artificial (such as small molecule based gelators) polymers. For example, recent studies have found that the assembly of microtubules is better explained as a combination of the lateral and longitudinal binding energies of tubulin, consistent with our model, rather than the classical helicoidal assembly model.[38] Moreover, the de-assembly or "catastrophe" following small conformational changes of the tubulin building blocks is also consistent with the all-or-nothing assembly following small changes in the individual pairwise binding constants,[6] as predicted by our model. Also consistent with our model, it has been observed that the degree of cooperativity in the assembly of some small molecule based gelators depends on the thickness of the gel fibres, which in turns depends on the number of strands that form the fibre.[20]

Our model does not exclude the possibility that other cooperative effects of allosteric origin may also play a role in supramolecular polymerization, especially for single-stranded polymers. However, this work shows that for multi-stranded polymers, multivalence cooperativity plays a central role that our model can describe quantitatively. For these polymers, the maximum number of strands m, together with the lateral and oligomerization constants are the key parameters that dictate the preferred size of the oligomer and the nucleation concentration. Since these parameters depend ultimately on the structure of the building blocks, our model is also a useful tool to predict the assembly properties of *de novo* synthesized molecules. We believe however that our interpretation of the all-or-nothing assembly of supramolecular polymers, whereby the chelate effect is triggered after a multivalent nucleus if formed, can be applied to the formation of any kind of long range assembly that follows a cooperative, all-or-nothing behaviour. Our model can therefore be expanded to include processes as diverse as the crystallization of small molecules or the formation of cell membrane adhesion points. Regarding the latter, previous work from our group has led to an analogous assembly model for membrane embedded receptors.[39,40] Current work in our laboratories is directed at demonstrating the general applicability of the model and the specific applicability to cell–cell communication processes involving cell membrane contacts and in the design of multi-stranded supramolecular polymers with predictable assembly properties.

Acknowledgements

We thank Dr Abil Aliev (Department of Chemistry, University College London) for his assistance in performing and analysing the DOSY NMR experiments. We thank the School of Sciences at Birkbeck, University of London, for funding. EM was performed at the School of Crystallography, Birkbeck University of London, supported by a Wellcome Trust program grant to Prof. Helen Saibil.

Notes and references

1 A. Whitty, *Nat. Chem. Biol.*, 2008, **4**, 435.
2 C. A. Hunter and H. L. Anderson, *Angew. Chem., Int. Ed.*, 2009, **48**, 7488.
3 M. Mammen, S.-K. Choi and G. M. Whitesides, *Angew. Chem., Int. Ed.*, 1998, **37**, 2754.
4 J. D. Badjic, A. Nelson, S. J. Cantrill, W. B. Turnbull and J. F. Stoddart, *Acc. Chem. Res.*, 2005, **38**, 723.
5 A. Mulder, J. Huskens and D. N. Reinhoudt, *Org. Biomol. Chem.*, 2004, **2**, 3409.
6 D. A. Fetcher and R. D. Mullinds, *Nature*, 2010, **463**, 285.
7 T. F. A. De Greef, M. M. J. Smulders, M. Wolffs, A. P. H. J. Schenning, R. P. Sijbesma and E. W. Meijer, *Chem. Rev.*, 2009, **109**, 5687.
8 T. Aida, S. I. Stupp and E. W. Meijer, *Science*, 2012, **335**, 813.
9 A. P. H. J. Schenning and E. W. Meijer, *Chem. Commun.*, 2005, 3245.
10 F. J. M. Hoeben, A. P. H. J. Schenning and E. W. Meijer, *ChemPhysChem*, 2005, **6**, 2337.
11 R. Abbel, C. Grenier, M. J. Pouderoijen, J. W. Stouwdam, P. E. L. G. Leclere, R. P. Sijbesma, E. W. Meijer and A. P. H. J. Schenning, *J. Am. Chem. Soc.*, 2009, **131**, 833.
12 L. Milanesi, C. A. Hunter, N. Tzokova, J. P. Waltho and S. Tomas, *Chem.–Eur. J.*, 2011, **17**, 9753.
13 E. J. Howe, B. O. Okesola and D. K. Smith, *Chem. Commun.*, 2015, 7451.
14 A. R. Hirst, B. Escuder, J. F. Miravet and D. K. Smith, *Angew. Chem., Int. Ed.*, 2008, **47**, 8002.
15 A. S. Weingarten, R. V. Kazantsev, L. C. Palmer, M. McClendon, A. R. Koltonow, A. P. S. Samuel, D. J. Kiebala, M. R. Wasielewski and S. I. Stupp, *Nat. Chem.*, 2014, **6**, 964.
16 R. N. Shah, N. A. Shah, M. M. D. Lim, C. Hsieh, G. Nuber and S. I. Stupp, *Proc. Natl. Acad. Sci. U. S. A.*, 2010, **107**, 3293.
17 G. A. Silva, C. Czeislszer, K. L. Niece, E. Beniash, D. A. Harrington, J. A. Kessler and S. I. Stupp, *Science*, 2004, **303**, 1352.
18 J. Boekhoven and S. I. Stupp, *Adv. Mater.*, 2014, **26**, 1642.
19 D. H. Zhao and J. S. Moore, *Org. Biomol. Chem.*, 2003, **1**, 3471.

20 A. R. Hirst, I. A. Coates, T. R. Boucheteau, J. F. Miravet, B. Escuder, V. Castelletto, I. W. Hamley and D. K. Smith, *J. Am. Chem. Soc.*, 2008, **130**, 9113.
21 R. Krishnan and S. L. Lindquist, *Nature*, 2005, **435**, 765.
22 S. L. Bernstein, N. F. Dupuis, N. D. Lazo, T. Wyttenbach, M. M. Condron, G. Bitan, D. B. Teplow, J.-E. Shea, B. T. Ruotolo, C. V. Robinson and M. T. Bowers, *Nat. Chem.*, 2009, **1**, 326.
23 P. A. Korevaar, S. J. George, A. J. Markvoort, M. M. J. Smulders, P. A. J. Hilbers, A. P. H. J. Schenning, T. F. A. De Greef and E. W. Meijer, *Nature*, 2012, **481**, 492.
24 P. Jonkheijm, P. van der Schoot, A. P. H. J. Schenning and E. W. Meijer, *Science*, 2006, **313**, 80.
25 F. Oosawa and M. Kasai, *J. Mol. Biol.*, 1962, **4**, 10.
26 E. D. Korn, *Physiol. Rev.*, 1982, **62**, 672.
27 H. L. Anderson, *Chem. Commun.*, 1999, 2323.
28 Y. Tian, C. M. Beavers, T. Busani, K. E. Martin, J. L. Jacobsen, B. Q. Mercado, B. S. Swartzentruber, F. van Swol, C. F. Medforth and J. A. Shelnutt, *Nanoscale*, 2012, **4**, 1695.
29 M. Gilbert and B. Albinsson, *Chem. Soc. Rev.*, 2015, **44**, 845.
30 C. A. Hunter and S. Tomas, *J. Am. Chem. Soc.*, 2006, **128**, 8975.
31 A. Camara-Campos, C. A. Hunter and S. Tomas, *Proc. Natl. Acad. Sci. U. S. A.*, 2006, **103**, 3034.
32 M. Bhatti, T. D. McHugh, L. Milanesi and S. Tomas, *Chem. Commun.*, 2014, 7649.
33 A. Ortega, D. Amoros and J. Garcia de la Torre, *Biophys. J.*, 2011, **101**, 892.
34 O. Ono, Y. Kaizu and H. Kobayashi, *J. Chem. Phys.*, 1993, **99**, 4128.
35 Y. Gao, X. Zhang, C. Ma, X. Li and J. Jiang, *J. Am. Chem. Soc.*, 2008, **130**, 17044.
36 A. Fidalgo-Marijuan, G. Barandika, B. Baza, M.-K. Urtiaga and M. I. Arriortua, *CrystEngComm*, 2013, **15**, 4181.
37 M. C. Misuraca, T. Grecu, Z. Freixa, V. Garavini, C. A. Hunter, P. W. van Leeuwen, M. D. Segarra-Maset and S. M. Turega, *J. Org. Chem.*, 2011, **76**, 2723.
38 M. K. Gardner, B. D. Charlebois, I. M. Jánosi, J. Howard, A. J. Hunt and D. J. Odde, *Cell*, 2011, **146**, 582.
39 S. Tomas and L. Milanesi, *Nat. Chem.*, 2010, **2**, 1077.
40 A. Grochmal, E. Ferrero, L. Milanesi and S. Tomas, *J. Am. Chem. Soc.*, 2013, **135**, 10172.